

Massive MIMO with Dense Arrays and 1-bit Data Converters

Amine Mezghani¹, *Member, IEEE*, Faouzi Bellili¹, *Member, IEEE*, and Robert W. Heath, Jr.², *Fellow, IEEE*

¹E2-390 E.I.T.C, 75 Chancellor's Circle, Winnipeg, MB, R3T 5V6, Canada.

²890 Oval Drive 3100 Engineering Building II, Raleigh, NC 27695, United States

Emails: {amine.mezghani,faouzi.bellili}@umanitoba.ca, rweathjr@ncsu.edu

Abstract—We consider wireless communication systems with compact planar arrays having densely spaced antenna elements in conjunction with one-bit analog-to-digital and digital-to-analog converters (ADCs/DACs). We provide closed-form expressions for the achievable rates with simple linear processing techniques for the uplink as well as the downlink scenarios while taking into account the effects of antenna mutual coupling. In the downlink case, we introduce the concept of non-radiating dithering to combat correlations of the quantization errors. Under higher antenna element density, we show that the performance of the quantized system can be made close to the ideal performance regardless of the operating signal-to-noise ratio.

Index Terms—Massive MIMO, Broadband antenna arrays, Tightly coupled antennas, Sub-wavelength oversampling, One-bit ADCs/DACs.

I. INTRODUCTION

The use of multi-antenna transmissions has shaped the wireless research and industry in the last two decades [1]. With the advent of massive multiple-input-multiple-output (massive MIMO) [2], high simultaneous multiplexing/diversity/array gains were made possible, thereby substantially improving energy and spectral efficiencies at the same time. Yet, several questions remain open: *i*) the development of multi-standard super-wideband base stations, *ii*) the realization of fully digital radio-frontend at millimeter-wave frequencies and above, and *iii*) the convergence of the radio technology into a unified platform [3].

Much like the physical-layer wireless technology, the antenna technology has evolved immensely and the current trend is moving toward ultrathin compact/conformal antenna surfaces with subwavelength (i.e., microscopic) structures, also known as metasurfaces with 2D applied/induced magnetic and electric currents along the surface [4]. These new designs will enable multipurpose reconfigurable active/passive radiators/scatterers that can operate at several frequencies and enable more than one functionality at the same time via full 3D (i.e., 360°) beamforming.

Conventional narrowband antenna arrays that are for instance still used in massive MIMO systems are generally based

on a discrete array architecture where the element spacing is in the order of a half-wavelength. Newer antenna concepts, such as metasurfaces and tightly coupled dipole arrays [5] are by contrast made of smaller elements with sub-wavelength spacing to synthesize a quasi-continuous aperture.

In the context of passive metasurfaces, the subwavelength structure offers a flexible and efficient wavefront manipulation such as beam-steering of the incident wave by optimizing the surface impedance distribution. There are many other reasons for which subwavelength oversampling of the aperture can be advantageous also in the case of active arrays. First, for wideband antenna and ultra-wideband arrays with tightly coupled elements [6], [7], the inter-element spacing should be equal or smaller than the minimum operating half-wavelength to avoid grating lobes, leading to inherent oversampling at the lower operating frequencies. Second, super-directivity [8] is possible with compact arrays albeit only at a small scale with an aperture size of few wavelengths due to the prohibitive losses and extreme narrowband behavior [9], [10]. Third, near-field communication based on evanescent non-propagating fields (and thus not limited by the diffraction limit) can be envisioned for certain applications such as chip-to-chip communications and brain implant data transfer offering high multiplexing gains and high-security standard [11].

Our work falls under the context of exploiting spatial oversampling to reduce the effects of nonlinear radio frontends, such as the quantization losses when low-resolution ADCs and DACs are used even down to just one-bit resolution per real dimension as a means to reduce implementation complexity and power consumption. This idea of trading simpler hardware for higher sampling in space has been already considered in prior work [12]–[16]. Indeed, the trend towards wideband arrays with subwavelength structures will make this coarse quantization concept even more attractive. Prior work, however, mainly focused on sigma-delta low-bit conversion that applies only for uniform linear arrays and necessitates sequential (i.e., non-parallelizable) processing.

A. Contributions

We derive bounds on the rate achievable with tightly coupled antenna arrays where the inter-element spacing is less than the half-wavelength for both the downlink as well as

A. Mezghani and F. Bellili are with the ECE Department at the University of Manitoba, Winnipeg, MB, Canada (emails: {Amine.Mezghani, Faouzi.Bellili}@umanitoba.ca). R. W. Heath is with the North Carolina State University (email: rweathjr@ncsu.edu). This work was supported by Discovery Grants Program of the Natural Sciences and Engineering Research Council of Canada (NSERC) and the US National Science Foundation (NSF).

the uplink cases under 1-bit data converters. To this end, we derive a model for the antenna array response as well as for the spatial noise correlations that takes into account the antenna coupling effects based on the law of power conservation. The lower bound on the achievable rate is obtained through the Busgang decomposition of the converters' output and by treating nonlinear distortion as additive noise.

For a fixed total antenna aperture, we show that, while the uplink and downlink system with infinite resolution ADCs and DACs do not benefit from the spatial oversampling, one-bit systems can substantially take advantage of the sub-wavelength sampling even with purely linear processing. To this end, we show the essential role of dithering applied prior to quantization to decorrelate the distortion error, a necessary feature to approach the ideal performance with linear processing. For the receiving arrays, dithering is performed naturally via the noise added by the low noise amplifiers (LNAs). For transmitting arrays, this can be achieved by intentionally adding digital non-radiating (reactive) noise to the digital transmit signal before the one-bit DAC.

Interestingly, since dithering can be fully controlled in the downlink case, one-bit transmitting arrays appear to asymptotically approach the ideal performance at zero loss, and regardless of the effective SNR, as the number of spatial oversampling factor grows large. In the case of dense receiving arrays, a non-zero, but SNR independent, gap to the ideal case persists due to the fact that the dither signal from the LNAs is natural and cannot be optimized. This is in contrast to the prior work [17]–[34] focusing on uncoupled antenna arrays and suggesting the effectiveness of mid-rise one-bit sampling only in the low to medium SNR regime with a minimum of $2/\pi$ SNR loss.

Through numerical examples, we illustrate our findings regarding the performance of dense arrays with 1-bit ADCs and DACs. We also draw conclusions on the power-efficient implementation of tightly spaced antenna arrays with one-bit DAC.

B. Notation

Vectors and matrices are denoted by lower and upper case italic bold letters. The operators $(\bullet)^T$, $(\bullet)^H$, $\text{tr}(\bullet)$ and $(\bullet)^*$ stand for transpose, Hermitian (conjugate transpose), trace, and complex conjugate, respectively. The term \mathbf{I}_M represents the identity matrix of size M . The vector \mathbf{x}_i denotes the i -th column of a matrix \mathbf{X} and $[\mathbf{X}]_{i,j}$ denotes the $(i$ th, j th) element, while x_i is the i -th element of the vector \mathbf{x} . We represent the Kronecker product of vectors and matrices by the operators " \otimes ". Additionally, $\text{Diag}(\mathbf{B})$ denotes a diagonal matrix containing only the diagonal elements of \mathbf{B} . Further, we define $\mathbf{C}_x = \mathbb{E}[\mathbf{x}\mathbf{x}^H] - \mathbb{E}[\mathbf{x}]\mathbb{E}[\mathbf{x}^H]$ as the covariance matrix of \mathbf{x} and \mathbf{C}_{xy} as $\mathbb{E}[\mathbf{x}\mathbf{y}^H]$.

II. DENSE ANTENNA ARRAY MODELS

The model for the dense antenna array used in this paper is in line with the prior work [8] and is based on power conservation arguments. We first derive a condition on any admissible model for densely spaced antenna architecture.

The condition implies certain limitations on the achievable embedded radiation pattern of the array elements. We then argue that the widely used cosine based radiation pattern complies with this condition.

A. Condition for power conservation at the far-field

Consider a quasi-continuous infinite unidirectional antenna surface with element far-field effective area (i.e., embedded pattern) $A_e(\theta, \varphi)$ for the elevation (aspect) and azimuth angles θ and φ for all element while neglecting the edge effects. The far-field array steering vector of an $\sqrt{M} \times \sqrt{M}$ uniform linear array is

$$\mathbf{a}(\theta, \varphi, f) = \begin{bmatrix} 1 \\ e^{-2\pi j \frac{a}{\lambda} \sin \theta \sin \varphi} \\ \vdots \\ e^{-2\pi j \frac{a}{\lambda} (\sqrt{M}-1) \sin \theta \sin \varphi} \end{bmatrix} \otimes \begin{bmatrix} 1 \\ e^{-2\pi j \frac{a}{\lambda} \sin \theta \cos \varphi} \\ \vdots \\ e^{-2\pi j \frac{a}{\lambda} (\sqrt{M}-1) \sin \theta \cos \varphi} \end{bmatrix}, \quad (1)$$

with a being the element spacing and λ is the wavelength.

When dealing with spatial oversampling, i.e., $a \leq \lambda/2$, it is crucial to distinguish between extrinsic (environmental) and intrinsic (device) noise sources. At environmental temperature T , the isotropic thermal radiation density for one polarization is given by

$$N_f(f, T) = \frac{hf^3}{c^2} \frac{1}{e^{hf/N_0} - 1} \stackrel{hf \ll N_0}{\approx} \frac{N_0}{\lambda^2}, \quad \lambda = c_0/f$$

where the approximation holds for the radio spectrum at ordinary temperatures. Consequently, the spatial covariance matrix associated with the environmental (i.e., extrinsic) noise is given by

$$\begin{aligned} \mathbf{C}_n(f) &= N_f(f, T) \int_0^{\frac{\pi}{2}} \int_{-\pi}^{\pi} A_e(\theta, \varphi) \mathbf{a}(\theta, \varphi, f) \mathbf{a}(\theta, \varphi, f)^H \sin \theta d\varphi d\theta \\ &= N_0 \int_0^{\frac{\pi}{2}} \int_{-\pi}^{\pi} \frac{1}{\lambda^2} A_e(\theta, \varphi) \mathbf{a}(\theta, \varphi, f) \mathbf{a}(\theta, \varphi, f)^H \sin \theta d\varphi d\theta \\ &\triangleq N_0 \mathbf{B}(f). \end{aligned} \quad (2)$$

We call the matrix $\mathbf{B}(f)$ the coupling matrix. Due to the Fourier structure of the array response in (1), one can notice that the matrix $\mathbf{B}(f)$ tend to be low rank in case of spatial oversampling with $a \ll \lambda$ and so does the extrinsic noise covariance matrix. This is due to the fact that $\mathbf{a}(\theta, \varphi, f)$ spans only a small portion of the M -dimensional space if $a \ll \lambda$. Based on the equipartition of energy principle, the average extrinsic energy associated with each complex degree of freedom received from the ambient environment cannot exceed N_0 , therefore we must have the property:

Result 1. Any time invariant antenna array fulfils $\mathbf{B}(f) \preceq \mathbf{I}$.

Proof. The coupling matrix $\mathbf{B}(f)$ is related to the antenna impedance \mathbf{Z} (or alternatively admittance matrix) by calculating the effective covariance of the noise delivered by the

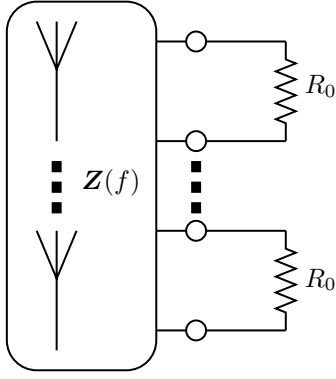


Fig. 1: Circuit diagram of a MIMO antenna system with resistive loads

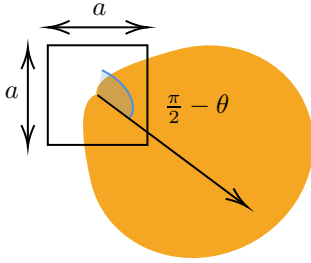


Fig. 2: Unit element of the array: for a cosine shaped pattern $A_e(\theta, \varphi) = a^2 \cos \theta$

antenna system to M resistive loads with value R_0 as shown in Fig. 1 [10], [35]

$$\mathbf{B}(f) = (R_0 \mathbf{I} + \mathbf{Z}(f))^{-1} 4\mathcal{R}\{\mathbf{Z}(f)\} R_0 (R_0 \mathbf{I} + \mathbf{Z}(f))^{-H}. \quad (3)$$

Then, we compare the denominator and numerator of the matrix fraction in (3)

$$\begin{aligned} (R_0 \mathbf{I} + \mathbf{Z}(f))(R_0 \mathbf{I} + \mathbf{Z}(f))^H - 4\mathcal{R}\{\mathbf{Z}(f)\} R_0 \\ = (R_0 \mathbf{I} - \mathbf{Z}(f))(R_0 \mathbf{I} - \mathbf{Z}(f))^H \succcurlyeq 0, \end{aligned} \quad (4)$$

leading to the property $\mathbf{B}(f) \preceq \mathbf{I}$. \square

A possible admissible effective area that is compatible with the passivity condition $\mathbf{B}(f) \preceq \mathbf{I}$ is the cosine-shaped pattern (know as the normal gain with uniformly illuminated aperture, c.f. Fig. 2)

$$A_e(\theta, \varphi) = a^2 \cos \theta. \quad (5)$$

A practical implementation using connected dipoles that

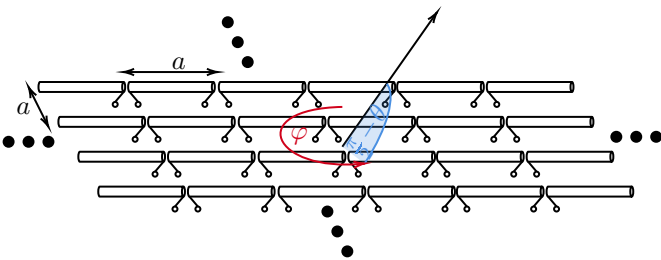


Fig. 3: Connected dipole array

approximately achieves this behavior can be found in [5] and is illustrated in Fig. 3.

Result 2. The cosine pattern $A_e(\theta, \varphi) = a^2 \cos \theta$ fulfils the condition $\mathbf{B}(f) \preceq \mathbf{I}$.

Proof. Taking the case that $A_e(\theta, \varphi) = a^2 \cos \theta$, we prove that $\mathbf{B}(f) \preceq \mathbf{I}$, which is equivalent to $\mathbf{f}^T \mathbf{B}(f) \mathbf{f}^* \leq \|\mathbf{f}\|_2^2, \forall \mathbf{f}$. To this end, we use the substitution

$$x = \frac{a}{\lambda} \sin \theta \cos \varphi \quad (6)$$

$$y = \frac{a}{\lambda} \sin \theta \sin \varphi. \quad (7)$$

Then, we evaluate the quadratic form

$$\begin{aligned} \mathbf{f}^T \mathbf{B}(f) \mathbf{f}^* &= \int_0^{\frac{\pi}{2}} \int_{-\pi}^{\pi} |\mathbf{f}^T \mathbf{a}(\theta, \varphi, f)|^2 \cos \theta \sin \theta d\varphi d\theta \\ &= \iint_{x^2 + y^2 \leq \frac{a^2}{\lambda^2}} |\mathbf{f}^T \tilde{\mathbf{a}}(x, y, f)|^2 dx dy \\ &\leq \int_{-\frac{1}{2}}^{\frac{1}{2}} \int_{-\frac{1}{2}}^{\frac{1}{2}} |\mathbf{f}^T \tilde{\mathbf{a}}(x, y, f)|^2 dx dy \\ &= \|\mathbf{f}\|_2^2 \quad (\text{Parseval's theorem}). \end{aligned} \quad (8)$$

\square

Explicitly, for the case with $A_e(\theta, \varphi) = a^2 \cos \theta$, the kernel matrix $\mathbf{B}(f)$ is obtained from the evaluation of the spherical integral in (2) as follows [8]

$$[\mathbf{B}(f)]_{k+\sqrt{M}(\ell-1), m+\sqrt{M}(n-1)} = \begin{cases} \frac{\pi a^2}{\lambda^2}, & \text{for } k = m \text{ and } \ell = n \\ \frac{a}{\lambda} \frac{J_1(\frac{2\pi a}{\lambda} \sqrt{(k-m)^2 + (\ell-n)^2})}{\sqrt{(k-m)^2 + (\ell-n)^2}}, & \text{otherwise,} \end{cases} \quad (9)$$

where $J_1(\bullet)$ is the Bessel function of first kind and first order. Finally, we also introduce the following quantity related to the diagonal entries of the matrix $\mathbf{B}(f)$

$$\gamma = \int_0^{\frac{\pi}{2}} \int_{-\pi}^{\pi} \frac{1}{a^2} A_e(\theta, \varphi) \sin \theta d\varphi d\theta = \frac{\lambda^2}{a^2} [\mathbf{B}(f)]_{j,j}, \quad (10)$$

which is equal π for the cosine pattern.

B. Receive array and noise correlation

Consider the case where the antenna array is operated in the receiving mode. The total effective noise is the sum of the contributions from environmental noise as characterized in (2), and the intrinsic noise of the device that is dominated usually by the noise sources of the low noise amplifier (LNA). Denoting the noise figure (i.e., the noise enhancement factor) of the LNA by N_F , and assuming uncorrelated device noise, we obtain using (2) the total noise covariance matrix

$$\begin{aligned} \mathbf{C}_{n, \text{Tot}}(f) &= N_0 \underbrace{\int_0^{\frac{\pi}{2}} \int_{-\pi}^{\pi} \frac{1}{\lambda^2} A_e(\theta, \varphi) \mathbf{a}(\theta, \varphi, f) \mathbf{a}(\theta, \varphi, f)^H \sin \theta d\varphi d\theta}_{\text{extrinsic noise}} \\ &\quad + \underbrace{(N_F - 1) N_0 \mathbf{I}}_{\text{device noise}} \\ &= N_0 \mathbf{B}(f) + (N_F - 1) N_0 \mathbf{I}, \end{aligned} \quad (11)$$

where $N_F > 1$ represents the noise figure of the receiver. The assumption of uncorrelated device noise, although being not exact, is quite reasonable and provide meaningful prediction of the performance as shown later. This uncorrelated intrinsic/device noise could also include the Ohmic losses of the antenna structure. Again, since $\mathbf{B}(f) \preceq \mathbf{I}$, we have $\mathbf{C}_{n,\text{Tot}}(f) \preceq N_F N_0 \mathbf{I}$.

C. Transmit array and radiated power

When operating as a transmit array, we use the following relationship between the element antenna pattern and its effective area which follows from thermodynamical arguments [36]

$$G_e(\theta, \varphi) = \frac{4\pi}{\lambda^2} A_e(\theta, \varphi). \quad (12)$$

When an excitation vector \mathbf{f} is applied to the antenna array, the total radiated power spectral density is obtained by integrating the radiated signal over a distance of 1 meter

$$\begin{aligned} \Phi_{R,\text{Tot}}(f) &= \frac{1}{4\pi} \int_0^{\frac{\pi}{2}} \int_{-\pi}^{\pi} G_e(\theta, \varphi) |\mathbf{f}^T \mathbf{a}(\theta, \varphi, f)|^2 \sin\theta d\varphi d\theta \\ &= \int_0^{\frac{\pi}{2}} \int_{-\pi}^{\pi} \frac{1}{\lambda^2} A_e(\theta, \varphi) |\mathbf{f}^T \mathbf{a}(\theta, \varphi, f)|^2 \sin\theta d\varphi d\theta \\ &= \mathbf{f}^T \mathbf{B}(f) \mathbf{f}^* \\ &\leq \|\mathbf{f}\|_2^2, \end{aligned} \quad (13)$$

where $\mathbf{B}(f)$ is defined in (2) and the last step follows from $\mathbf{B}(f) \preceq \mathbf{I}$. The radiated power is less or equal the available power $\|\mathbf{f}\|_2^2$ and the equality holds only in the case $\mathbf{B}(f) = \mathbf{I}$, i.e., with perfect impedance matching conditions. The radiation pattern $\mathbf{f}^T \mathbf{a}(\theta, \varphi, f)$ is the truncated discrete-space Fourier transform (DTFT) of the beamforming vector \mathbf{f} . We notice therefore the spatial smoothing and filtering property of dense antenna array, as only the lowest spatial frequencies $x^2 + y^2 \leq \frac{a^2}{\lambda^2} \leq 1$ can propagate. Thus, spatial oversampling enables the reduction – with a 2D cylindrical filter shape in the case of the cosine pattern (c.f. (8))– of potential spurious radiations in the beamforming vector \mathbf{f} due for instance to hardware impairments. Since only the lower angular frequencies $x^2 + y^2 \leq \frac{a^2}{\lambda^2} \leq 1$ can be radiated, any excitation outside this band will just generate reactive power that remains stored and confined very close (within few wavelengths) to the array surface. Consequently, constant envelope transmission as well as low resolution D/A-converters can be used more appropriately in combination with densely spaced antenna arrays as suggested in prior work [15].

D. Far-field channel model

Consider K users in the far-field of the antenna array. The individual channels (assumed to be narrowband for simplicity) can be written a superposition of Q multi-path components

$$\mathbf{h}_k = \sum_{\ell=1}^Q s'_\ell \frac{1}{\lambda} \sqrt{A_e(\theta_\ell, \varphi_\ell)} \mathbf{a}(\theta_\ell, \varphi_\ell, f), \quad (14)$$

where $f = 2\pi/\lambda$ is the carrier frequency. In case of Rayleigh fading, i.e., rich scattering scenarios with isotropic angles

of arrivals (for the uplink scenario) or departures (for the downlink scenario), the vector \mathbf{s}_k becomes independent and identically distributed (IID) Gaussian. In such a case, the channel covariance matrix is equal to $\mathbf{B}(f)$ (c.f. (2))

$$\mathbb{E}[\mathbf{h}_k, \mathbf{h}_k^H] = \mathbf{B}(f). \quad (15)$$

Accordingly, we can represent the channel vectors in the image space spanned by the matrix $\mathbf{B}(f)$

$$\mathbf{h}_k = \mathbf{B}(f)^{\frac{1}{2}} \mathbf{s}_k, \quad (16)$$

with IID complex Gaussian vectors \mathbf{s}_k . This shows again the significance of the coupling matrix $\mathbf{B}(f)$ for the overall system model.

III. SPECTRAL EFFICIENCY WITH ZERO-FORCING RECEIVER AND ONE-BIT RESOLUTION ADCs

We first consider the achievable rate infinite resolution ADCs and zero-forcing detection. The received signal is

$$\mathbf{y} = \mathbf{H}\mathbf{x} + \mathbf{n}, \quad (17)$$

where \mathbf{n} is the effective noise vector having the covariance matrix given in (11), $\mathbf{x} \in \mathbb{C}^K$ is the signal vector containing the transmitted signals from all the users with individual power values ε_k , and the channel matrix is defined as

$$\mathbf{H} = [\mathbf{h}_1, \dots, \mathbf{h}_K]. \quad (18)$$

The individual achievable rates based on zero-forcing equalizer

$$\mathbf{G} = (\mathbf{H}^H \mathbf{H})^{-1} \mathbf{H}^H, \quad (19)$$

are given by

$$\begin{aligned} R_k &= \log_2 \left(1 + \frac{\varepsilon_k}{[(\mathbf{H}^H \mathbf{C}_{n,\text{Tot}}^{-1} \mathbf{H})^{-1}]_{kk}} \right) \\ &= \log_2 \left(1 + \frac{\varepsilon_k / N_0}{[(\mathbf{S}^H (\mathbf{I} + (N_F - 1) \mathbf{B}(f)^{-1} \mathbf{S}))^{-1}]_{kk}} \right). \end{aligned} \quad (20)$$

Since the matrix $\mathbf{B}(f)$ is dominated by about $\frac{4a^2}{\lambda^2} M$ eigenvalues [8], [37] and N_f is strictly larger than 1, the rate in a linear system mainly depends on the effective aperture $\frac{4a^2}{\lambda^2} M$ rather than the number of antenna elements M in dense arrays. In other words, half-wavelength spacing, i.e., $a = \lambda/2$, is nearly optimal in large antenna arrays with infinite resolution ADCs. This fact will be also apparent in the numerical results.

For the 1-bit case, shown in Fig. 4, we resort to the Bussgang decomposition technique to derive a lower bound on the achievable rate. The rescaled quantized output is

$$\mathbf{y}_Q = \frac{\mathbf{D}^{\frac{1}{2}}}{\sqrt{2}} (\text{sign}(\mathcal{R}(\mathbf{y})) + j \cdot \text{sign}(\mathcal{I}(\mathbf{y}))). \quad (21)$$

where \mathbf{D} is a diagonal matrix containing the diagonal entries of \mathbf{C}_y

$$\mathbf{C}_y = \mathbf{H} \mathbf{P} \mathbf{H}^H + \mathbf{C}_{n,\text{Tot}}, \quad \mathbf{P} = \begin{bmatrix} \varepsilon_1 & \cdots & 0 \\ \vdots & \ddots & \vdots \\ 0 & \cdots & \varepsilon_K \end{bmatrix}. \quad (22)$$

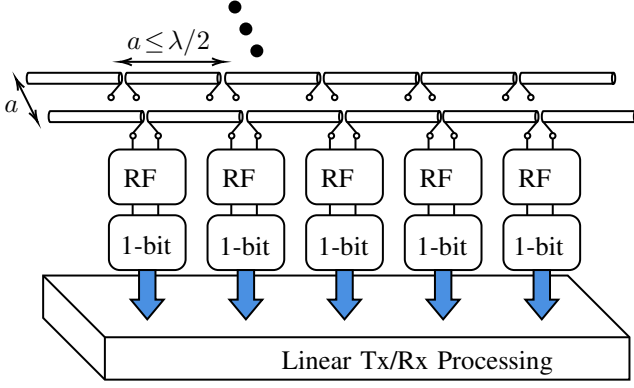


Fig. 4: Dense massive MIMO with 1-bit converters

The *arcsine law* provides first the relationship between covariance matrix at the input of the quantizer and the covariance matrix of quantized rescaled output

$$\begin{aligned} \mathbf{C}_{y_Q} &= \frac{2}{\pi} \mathbf{D}^{\frac{1}{2}} \arcsin \left(\mathbf{D}^{-\frac{1}{2}} \mathcal{R}(\mathbf{C}_y) \mathbf{D}^{-\frac{1}{2}} \right) \mathbf{D}^{\frac{1}{2}} \\ &+ j \frac{2}{\pi} \mathbf{D}^{\frac{1}{2}} \arcsin \left(\mathbf{D}^{-\frac{1}{2}} \mathcal{I}(\mathbf{C}_y) \mathbf{D}^{-\frac{1}{2}} \right) \mathbf{D}^{\frac{1}{2}}, \end{aligned} \quad (23)$$

where the arcsine function is applied elementwise. The effective noise covariance matrix can be obtained by subtracting the desired linear part of the Bussgang decomposition

$$\mathbf{C}'_{n, \text{Tot}} = \mathbf{C}_{y_Q} - \frac{2}{\pi} \mathbf{H} \mathbf{P} \mathbf{H}^H, \quad (24)$$

which includes contributions from both the additive noise as well as from the quantization distortion.

To further simplify the analysis, we resort to the following approximation under the assumption of small mutual correlations between the element signals

$$\mathbf{C}'_{n, \text{Tot}} \approx \left(1 - \frac{2}{\pi}\right) \mathbf{D} + \frac{2}{\pi} \mathbf{C}_{n, \text{Tot}}. \quad (25)$$

where we used the first order approximation

$$\arcsin(x) \approx \begin{cases} \frac{\pi}{2}, & \text{for } x = 1 \\ x, & \text{for } |x| < 1. \end{cases} \quad (26)$$

This approximation leads to uncorrelated quantization noise (UQN) which is widely used in the literature. It holds however only if the covariance matrix \mathbf{C}_y is dominantly diagonal. In other words, this approximation holds when the device noise dominates each individual element signal.

It is worth mentioning that the diagonal approximation assuming uncorrelated quantization noise might be unreasonable as shown in [38] but can be made more realistic with sufficiently lower SNR per antenna (e.g. $\frac{\alpha^2}{\lambda^2} \ll 1$). A lower bound on the mutual information [39] can be obtained by treating the distortion term as additive noise

$$\begin{aligned} R_{k, \text{LB}}^{1\text{-bit}} &= \log_2 \left(1 + \frac{\varepsilon_k}{\left[\left(\frac{2}{\pi} \mathbf{H}^H \mathbf{C}'_{n, \text{Tot}} \mathbf{H} \right)^{-1} \right]_{kk}} \right) \\ &\stackrel{\text{UQN}}{\approx} \log_2 \left(1 + \frac{\varepsilon_k}{\left[\mathbf{H}^H \left(\mathbf{C}_{n, \text{Tot}} + \left(\frac{\pi}{2} - 1 \right) \mathbf{D} \right)^{-1} \mathbf{H} \right]_{kk}} \right). \end{aligned} \quad (27)$$

In the case of large number of isotropically distributed users, we can make approximate the diagonal scaling matrix \mathbf{D} , i.e., the diagonal entries of the covariance matrix \mathbf{C}_y , as

$$\begin{aligned} \mathbf{D} &\approx \left(N_0 + \sum_k \varepsilon_k \right) \text{Diag}(\mathbf{B}(f)) + N_0(N_F - 1) \\ &= \left((N_0 + \sum_k \varepsilon_k) \frac{a^2}{\lambda^2} \underbrace{\int_0^{\frac{\pi}{2}} \int_{-\pi}^{\pi} A_e(\theta, \varphi) \sin \theta d\varphi d\theta}_{\triangleq \gamma (= \pi \text{ for the cosine pattern})} + N_0(N_F - 1) \right) \mathbf{I} \\ &= \left((N_0 + \sum_k \varepsilon_k) \frac{a^2}{\lambda^2} \gamma + N_0(N_F - 1) \right) \mathbf{I}. \end{aligned} \quad (28)$$

We obtain therefore the approximation

$$R_{k, \text{LB}}^{1\text{-bit}} \stackrel{\text{UQN}}{\approx} \log_2 \left(1 + \frac{\varepsilon_k / N_0}{\left[\left(\mathbf{S}^H \left(\mathbf{I} + \left(\frac{\pi}{2} (N_F - 1) + \left(\frac{\pi}{2} - 1 \right) \frac{a^2 \gamma}{\lambda^2} \left(1 + \sum_k \frac{\varepsilon_k}{N_0} \right) \right) \mathbf{B}(f)^{-1} \right)^{-1} \mathbf{S} \right]_{kk}} \right)}. \quad (29)$$

Now we state the following asymptotic result.

Result 3. For infinitely dense arrays, the SNR loss factor due the 1-bit quantization is

$$\lim_{\alpha \rightarrow 0} \frac{2^{R_{k, \text{LB}}^{1\text{-bit}}} - 1}{2^{R_k} - 1} = \frac{N_F}{1 + \frac{\pi}{2} (N_F - 1)}. \quad (30)$$

Interestingly, the ratio can be made close to one if the noise figure of the receivers chains N_F is close to one (i.e., nearly ideal receiver chain). Note that this result is independent of the SNRs ε_k / N_0 as opposed to the well-know $2/\pi$ loss factor [17], [38], [39] with uncoupled antennas that requires operating at sufficiently low SNR.

IV. SPECTRAL EFFICIENCY WITH ZERO-FORCING RECEIVER AND ONE-BIT DACS

Consider the ideal downlink case with infinite resolution DACs. The channel matrix can be represented as

$$\mathbf{H} = \mathbf{S} \mathbf{B}(f)^{\frac{1}{2}}. \quad (31)$$

At the base station, linear precoding with the matrix $\mathbf{F} \in \mathbb{C}^{K \times M}$ is applied to the symbol vector \mathbf{x} of the users and the signal received at the users stations is

$$\mathbf{r} = \mathbf{H} \mathbf{F} \mathbf{x} + \mathbf{n}. \quad (32)$$

As linear transmit processing, we take the widely used zero-forcing precoder which is given by

$$\mathbf{F} = \sqrt{\frac{\varepsilon}{\text{tr}((\mathbf{H} \mathbf{H}^H)^{-1})}} \mathbf{H}^H (\mathbf{H} \mathbf{H}^H)^{-1}, \quad (33)$$

where ε represents the total available power for transmission. The actual radiated power is however smaller than ε

$$\begin{aligned} P_R &= \frac{\text{tr}(\mathbf{H} \mathbf{B}(f) \mathbf{H}^H (\mathbf{H} \mathbf{H}^H)^{-2})}{\text{tr}((\mathbf{H} \mathbf{H}^H)^{-1})} \varepsilon \\ &= \frac{\text{tr}(\mathbf{S} \mathbf{B}(f)^2 \mathbf{S}^H (\mathbf{S} \mathbf{B}(f) \mathbf{S}^H)^{-2})}{\text{tr}((\mathbf{S} \mathbf{B}(f) \mathbf{S}^H)^{-1})} \varepsilon \leq \varepsilon \end{aligned} \quad (34)$$

where the inequality is due to $\mathbf{B}(f) \preceq \mathbf{I}$ and holds with equality for uncoupled antennas. In other words, only a portion of the available power ε is radiated. Furthermore, the achievable rate under the zero-forcing precoder can be written as

$$\begin{aligned} \bar{R}_k &= \log_2 \left(1 + \frac{\varepsilon/N_0/N_F}{\text{tr}((\mathbf{H}\mathbf{H}^H)^{-1})} \right) \\ &= \log_2 \left(1 + \frac{\varepsilon/N_0/N_F}{\text{tr}((\mathbf{S}\mathbf{B}(f)\mathbf{S}^H)^{-1})} \right). \end{aligned} \quad (35)$$

The use of densely space antenna transmit arrays in combination with low resolution DACs and sigma-delta conversion has been already considered in the literature, albeit only for the case of uniform linear arrays [12]–[16]. A generalization to be applied for planar arrays is rather not straightforward due the sequential precoding. Instead, we will use the technique of dithering [40], [41] to whiten the quantization error by adding a random signal prior to the 1-bit quantizer. Furthermore, to avoid injecting interference in the environments, we propose the concept of non-radiating dithering, where the dither signal lies mainly on the null space of the coupling matrix $\mathbf{B}(f)$. To minimize the radiated power originating from the additive dithering signal, we consider a matrix \mathbf{U} describing the approximate null space [42] of the coupling matrix¹ $\mathbf{B}(f)$, i.e.,

$$\text{tr}(\mathbf{U}^H \mathbf{B}(f) \mathbf{U}) / \text{tr}(\mathbf{U}^H \mathbf{U}) \ll 1. \quad (36)$$

Then, the dithering is performed after linear precoding as follows

$$\mathbf{z} = \mathbf{F}\mathbf{x} + \frac{\mathbf{U}}{\|\mathbf{U}\|_F} \mathbf{v}_d \quad (37)$$

with Gaussian IID dithering vector \mathbf{v}_d having variance σ_d^2 . A possible choice for \mathbf{U} is a projection on the approximate null space

$$\mathbf{U} = \mathbf{I} - (1 + \delta) \mathbf{B}(f)^{\frac{1}{2}} (\mathbf{B}(f) + \delta \mathbf{I})^{-1} \mathbf{B}(f)^{\frac{1}{2}}, \quad (38)$$

for sufficiently small δ which is used for as a threshold for the eigenvalues of $\mathbf{B}(f)$. Subsequently, the quantized transmit vector is given by

$$\mathbf{z}_Q = \sqrt{\alpha} \frac{\mathbf{D}^{\frac{1}{2}}}{\sqrt{2}} (\text{sign}(\mathcal{R}(\mathbf{z})) + \mathbf{j} \cdot \text{sign}(\mathcal{I}(\mathbf{z}))) \quad (39)$$

where a scaling factor α is introduced to ensure the same radiated power P_R as the ideal system. The rescaling matrix \mathbf{D} contains the diagonal elements of the covariance matrix of \mathbf{z}

$$\begin{aligned} \mathbf{D} &= \text{Diag}(\mathbf{F}\mathbf{F}^H + \frac{\mathbf{U}\mathbf{U}^H}{\|\mathbf{U}\|_F^2} \sigma_d^2) \\ &= \text{Diag}(\mathbf{F}\mathbf{F}^H + \frac{\sigma_d^2}{M} \mathbf{I}) \\ &\approx \frac{\varepsilon + \sigma_d^2}{M} \mathbf{I}, \end{aligned} \quad (40)$$

where the approximation holds for large number of users. With this approximation and assuming uncorrelated quantization

¹ $\mathbf{B}(f)$ is an "almost" low-rank matrix for $a \ll \lambda$ with many small eigenvalues but not exactly low-rank. Therefore a matrix \mathbf{U} is constructed that is nearly orthogonal to $\mathbf{B}(f)$.

noise, the radiated power of the 1-bit system has the following expression

$$\begin{aligned} P_R^{1\text{-bit}} &= \alpha \frac{2}{\pi} P_R + \alpha \text{tr}(\mathbf{D}^{\frac{1}{2}} \mathbf{R}_q \mathbf{D}^{\frac{1}{2}} \mathbf{B}(f)) \\ &\approx \alpha \frac{2}{\pi} P_R + \underbrace{\alpha \left(1 - \frac{2}{\pi}\right) \frac{a^2}{\lambda^2} (\varepsilon + \sigma_d^2) \gamma}_{\text{unwanted isotropic radiation}} \end{aligned} \quad (41)$$

To allow for a fair comparison, we equate the radiated power of the 1-bit system to the ideal system, $P_R^{1\text{-bit}} = P_R$, yielding

$$\alpha = \frac{P_R}{\frac{2}{\pi} P_R + \left(1 - \frac{2}{\pi}\right) \frac{a^2}{\lambda^2} (\varepsilon + \sigma_d^2) \gamma}. \quad (42)$$

Consequently, the noiseless received signal at the users terminals is

$$\mathbf{H}\mathbf{z}_Q = \sqrt{\alpha} \frac{2}{\pi} \frac{\varepsilon}{\text{tr}((\mathbf{H}\mathbf{H}^H)^{-1})} \mathbf{x} + \sqrt{\alpha} \mathbf{H} \mathbf{D}^{\frac{1}{2}} \mathbf{q}. \quad (43)$$

Finally, a lower bound on the achievable rate with 1-bit DACs can be obtained by simply modeling the quantization error as additive noise that is received through the channel

$$\begin{aligned} \bar{R}_{k,\text{LB}}^{1\text{-bit}} &= \log_2 \left(1 + \frac{\frac{2}{\pi} \alpha \varepsilon / \text{tr}((\mathbf{H}\mathbf{H}^H)^{-1})}{N_0 N_F + \alpha [\mathbf{H} \mathbf{D}^{\frac{1}{2}} \mathbf{R}_q \mathbf{D}^{\frac{1}{2}} \mathbf{H}^H]_{kk}} \right) \\ &\stackrel{\text{UQN}}{\approx} \log_2 \left(1 + \frac{\frac{2}{\pi} \alpha \varepsilon / \text{tr}((\mathbf{H}\mathbf{H}^H)^{-1})}{N_0 N_F + \alpha \left(1 - \frac{2}{\pi}\right) \frac{a^2}{\lambda^2} (\varepsilon + \sigma_d^2) \gamma} \right) \\ &= \log_2 \left(1 + \frac{\frac{2}{\pi} \alpha \varepsilon / \text{tr}((\mathbf{H}\mathbf{H}^H)^{-1})}{N_0 N_F + \left(1 - \frac{2}{\pi}\right) \varepsilon} \right) \\ &= \log_2 \left(1 + \frac{\varepsilon / \text{tr}((\mathbf{H}\mathbf{H}^H)^{-1}) / (N_0 N_F)}{1 + \left(\frac{1}{P_R} + \frac{1}{N_0 N_F}\right) \left(\frac{\pi}{2} - 1\right) \frac{a^2}{\lambda^2} (\varepsilon + \sigma_d^2) \gamma} \right). \end{aligned} \quad (44)$$

By comparing with the ideal case in (35), we state the following result.

Result 4. *For infinitely dense arrays, the SNR loss factor due the 1-bit DACs vanishes under the same radiated power as the ideal system*

$$\lim_{a \rightarrow 0} \frac{2^{\bar{R}_{k,\text{LB}}^{1\text{-bit}}} - 1}{2^{\bar{R}_k} - 1} = 1. \quad (45)$$

Interestingly, this results is better than Result 3 obtained for the uplink case with 1-bit ADCs. This can be explained by the fact that the additive dithering noise can be engineered in the DAC case, while the device noise for the ADC case is in general white and does not offer as much flexibility. It is worth mentioning that the choice of the dither variance σ_d^2 is critical. It has to be large enough to reduce the quantization noise correlation but excessive values would lead to a penalty as shown in the rate formula (44). This trade-off and the corresponding optimization of σ_d^2 have been considered for the case of conventional antenna arrays in [40], [41]. In our setting, the optimal value for σ_d^2 will depend on the number of users, antennas, and antenna spacing.

V. NUMERICAL EXAMPLES

We consider in this section some numerical examples and particular cases. In particular, we will discuss the validity of the common approximation of uncorrelated distortion error and draw key properties of densely spaced antenna systems with low-resolution converters. In fact, the validity of this approximation will also indicate how close the performance is to the ideal system when relying on simple linear processing [38].

In all numerical examples, we fix the total geometric aperture to be $a\sqrt{M} \times a\sqrt{M} = 2.5\lambda \times 2.5\lambda$, while varying M and a . Furthermore, we assume a cosine-based element pattern $A_e(\theta, \varphi) = a^2 \cos \theta$ since it is physically feasible. In addition, we consider a rich scattering environment with $K = 2$ users and isotropic multipath components, leading to a user's channel covariance matrix that is equal to $\mathbb{E}[\mathbf{h}_k \mathbf{h}_k^H] = \mathbf{B}(f)$. Accordingly, the performance results are averaged over 100 channel realizations.

A. Uplink case

Consider first the uplink case with $\varepsilon_k/N_0 = 2$ for both users and $N_F = 2$. The corresponding achievable rates are shown in Fig. 5 versus the number elements for the ideal case with infinite resolution as well as the one-bit case, both with and without the uncorrelated quantization noise assumption (UQN). The element count is increased from $M = 25$ ($\lambda/2$ inter-element spacing) to $M = 400$ ($\lambda/8$ inter-element spacing). The ideal system does not significantly take advantage of increasing the element density above half-wavelength spacing and the performance is mainly given by the total physical aperture. In fact, array gain beyond the normal geometric aperture of the antenna is known as super-gain but occurs practically only at small to moderate electrical size $\sqrt{2M} \frac{a}{\lambda}$ [9] and requires, in general, a matching network [10]. By contrast, the system with 1-bit ADCs clearly benefits from spatial oversampling and a substantial gain is obtained particularly when moving from $\lambda/2$ inter-element spacing to $\lambda/4$ inter-element spacing. We also observe that the UQN model tends to overpredict the performance particularly for $M = 25$, i.e., $a = \lambda/2$ but the discrepancy to the exact bound decreases as we increasingly overpopulate the antenna structure. This shows that ideal performance can be approached with 1-bit ADCs simple linear processing, without the need for complex spatial sigma-delta conversion as proposed in the prior work.

B. Downlink case

In the downlink scenario, a quite similar system setting is considered with 2 users and a rich scattering environment. We fix the available power to be $\varepsilon/(N_0 N_F) = 2$ and the total aperture to be $2.5\lambda \times 2.5\lambda$ and vary the number of elements from 25 up to 400. Again, the achievable rate of the ideal system hardly changes as shown in Fig. 6 for similar reasons as for the uplink case. Furthermore, the 1-bit system performs poorly if no dithering is introduced (dashed line) and does hardly improve with higher antenna count. This is explained by the strong correlations among the individual distortion

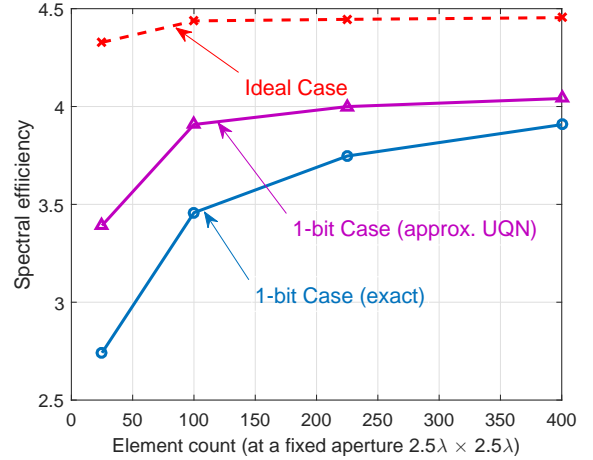


Fig. 5: Spectral efficiency versus element count for the uplink scenario at fixed aperture $2.5\lambda \times 2.5\lambda$ with $\varepsilon_k/N_0 = 2$, $N_F = 2$, and two users.

errors that combine coherently across the antenna/channel and severely affect the effective signal-to-noise-and-distortion ratio. In such a case, it is important to avoid the risk of relying on the oversimplified UQN model that might lead to misleading insights. Nevertheless, by adding non-radiating dithering according to (37) and (38), the performance improves substantially and the UQN becomes more accurate as shown in Fig. 6. To ensure this, the power of the dither signal σ_d^2 is increased proportionally to $\frac{\lambda}{a}$ to ensure the UQN property. Since this increase is still slower than $\frac{\lambda^2}{a^2}$, the performance derived in (44) can still arbitrarily approach the ideal performance. Fig. 7 illustrates the ratio of the radiated power P_R to power of the excitation vector, being ε for the ideal system and $\alpha(\varepsilon + \sigma_d^2)$ for the 1-bit system. The fact that the ratio for the 1-bit system reduces with the number of elements means that most of the power that circulates in the antenna is reactive in this regime. Since constant-envelope low-resolution signals are exciting the elements, this suggests the use of efficient switched-mode amplifiers exploiting the capability of the array for storing and recycling reactive power present in the evanescent field.

VI. CONCLUSION

Compact antenna arrays with inter-element spacing smaller than a half-wavelength are required for future radio systems to operate in different frequency bands and serve several applications and functionalities. We provided some requirements on any models used for this type of antennas to be physically consistent. Additionally, we showed that tightly spaced multiantenna systems can help to relax the linearity requirement of the radio frontend by using 1-bit converters and exploiting their spatial filtering feature provided by nature and at no extra digital processing complexity. In particular, power amplifiers can be operated in saturated or switched-mode, while most of the generated distortion manifests as evanescent-wave and does not radiate. This opens new directions for

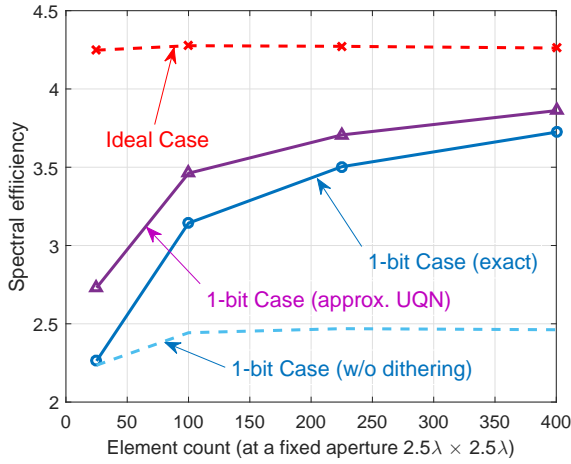


Fig. 6: Spectral efficiency versus element count for the downlink scenario at fixed aperture $2.5\lambda \times 2.5\lambda$ with $\varepsilon/(N_0N_F) = 2$, $\frac{\sigma_d^2}{\varepsilon} = \frac{\lambda}{3a}$, $\delta = 0.01$ and two users.

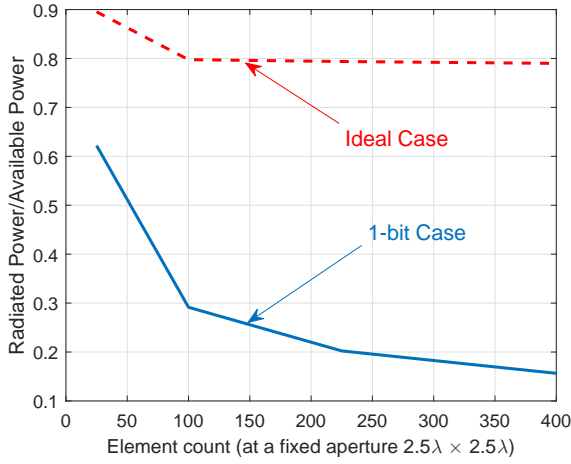


Fig. 7: Ratio P_R/ε in the ideal system and $P_R/(\alpha\varepsilon + \alpha\sigma_d^2)$ in the 1-bit system versus element count for the downlink scenario at fixed aperture $2.5\lambda \times 2.5\lambda$ with $\varepsilon/(N_0N_F) = 2$, $\frac{\sigma_d^2}{\varepsilon} = \frac{\lambda}{3a}$, $\delta = 0.01$ and two users.

designing waveforms and processing techniques dedicated to this type of antenna structures.

REFERENCES

- [1] R. W. Heath Jr and A. Lozano, *Foundations of MIMO communication*. Cambridge University Press, 2018.
- [2] T. L. Marzetta, "Noncooperative Cellular Wireless with Unlimited Numbers of Base Station Antennas," *IEEE Transactions on Wireless Communications*, vol. 9, no. 11, pp. 3590–3600, November 2010.
- [3] R. Thomä *et al.*, "Cooperative passive coherent location: A promising 5g service to support road safety," *arXiv*, July 2019.
- [4] M. D. Renzo, A. Zappone, M.-S. A. Merouane Debbah, C. Yuen, J. de Rosny, and S. Tretyakov, "Smart Radio Environments Empowered by Reconfigurable Intelligent Surfaces: How it Works, State of Research, and Road Ahea," *arXiv*, April 2020.
- [5] A. Neto and J. J. Lee, "Ultrawide-band properties of long slot arrays," *IEEE Transactions on Antennas and Propagation*, vol. 54, no. 2, pp. 534–543, 2006.
- [6] M. Jones and J. Rawnick, "A New Approach to Broadband Array Design using Tightly Coupled Elements," in *MILCOM 2007 - IEEE Military Communications Conference*, October 2007, pp. 1–7.

- [7] W. F. Moulder, K. Sertel, and J. L. Volakis, "Superstrate-Enhanced Ultrawideband Tightly Coupled Array With Resistive FSS," *IEEE Transactions on Antennas and Propagation*, vol. 60, no. 9, pp. 4166–4172, September 2012.
- [8] R. J. Williams, E. D. Carvalho, and T. L. Marzetta, "A Communication Model for Large Intelligent Surfaces," *arXiv 1912.06644*, 2019.
- [9] R. F. Harrington, "Effect of antenna size on gain, bandwidth, and efficiency," *J. Res. Nat. Bureau Stand.*, vol. 64D, pp. 1–12, January 1960.
- [10] M. T. Ivrlač and J. A. Nossek, "Toward a Circuit Theory of Communication," *IEEE Transactions on Circuits and Systems I: Regular Papers*, vol. 57, no. 7, pp. 1663–1683, July 2010.
- [11] S. Phang, M. T. Ivrlač, G. Gradoni, S. C. Creagh, G. Tanner, and J. A. Nossek, "Near-field mimo communication links," *IEEE Transactions on Circuits and Systems I: Regular Papers*, vol. 65, no. 9, pp. 3027–3036, 2018.
- [12] H. Pirzadeh, G. Seco-Granados, A. L. Swindlehurst, and J. A. Nossek, "On the Effect of Mutual Coupling in One-Bit Spatial Sigma-Delta Massive MIMO Systems," 2020.
- [13] D. S. Palguna, D. J. Love, T. A. Thomas, and A. Ghosh, "Millimeter Wave Receiver Design Using Low Precision Quantization and Parallel $\Delta\Sigma$ Architecture," *IEEE Transactions on Wireless Communications*, vol. 15, no. 10, pp. 6556–6569, 2016.
- [14] D. P. Scholnik, J. O. Coleman, D. Bowling, and M. Neel, "Spatio-temporal delta-sigma modulation for shared wideband transmit arrays," in *Proceedings of the 2004 IEEE Radar Conference (IEEE Cat. No. 04CH37509)*, 2004, pp. 85–90.
- [15] J. D. Krieger, C. Yeang, and G. W. Wornell, "Dense Delta-Sigma Phased Arrays," *IEEE Transactions on Antennas and Propagation*, vol. 61, no. 4, pp. 1825–1837, 2013.
- [16] M. Shao, W. Ma, Q. Li, and A. L. Swindlehurst, "One-Bit Sigma-Delta MIMO Precoding," *IEEE Journal of Selected Topics in Signal Processing*, vol. 13, no. 5, pp. 1046–1061, 2019.
- [17] A. Mezghani, M. S. Khoufi, and J. A. Nossek, "A Modified MMSE Receiver for Quantized MIMO Systems," *ITG WSA, Vienna, Austria*, February 2007.
- [18] A. Mezghani and J. A. Nossek, "On Ultra-Wideband MIMO Systems with 1-bit Quantized Outputs: Performance Analysis and Input Optimization," in *2007 IEEE International Symposium on Information Theory*, June 2007, pp. 1286–1289.
- [19] —, "Analysis of Rayleigh-fading channels with 1-bit quantized output," in *2008 IEEE International Symposium on Information Theory*, July 2008, pp. 260–264.
- [20] —, "Analysis of 1-bit output noncoherent fading channels in the low SNR regime," in *2009 IEEE International Symposium on Information Theory*, June 2009, pp. 1080–1084.
- [21] T. Koch and A. Lapidoth, "At Low SNR, Asymmetric Quantizers are Better," *IEEE Transactions on Information Theory*, vol. 59, no. 9, pp. 5421–5445, September 2013.
- [22] A. Mezghani, F. Antreich, and J. A. Nossek, "Multiple parameter estimation with quantized channel output," in *2010 International ITG Workshop on Smart Antennas (WSA)*, February 2010, pp. 143–150.
- [23] T. Koch and A. Lapidoth, "Increased capacity per unit-cost by oversampling," in *2010 IEEE 26-th Convention of Electrical and Electronics Engineers in Israel*, November 2010, pp. 684–688.
- [24] J. Mo and R. W. Heath, "Capacity Analysis of One-Bit Quantized MIMO Systems With Transmitter Channel State Information," *IEEE Transactions on Signal Processing*, vol. 63, no. 20, pp. 5498–5512, October 2015.
- [25] C. Studer and G. Durisi, "Quantized Massive MU-MIMO-OFDM Uplink," *IEEE Transactions on Communications*, vol. 64, no. 6, pp. 2387–2399, June 2016.
- [26] S. Jacobsson, G. Durisi, M. Coldrey, U. Gustavsson, and C. Studer, "Throughput Analysis of Massive MIMO Uplink With Low-Resolution ADCs," *IEEE Transactions on Wireless Communications*, vol. 16, no. 6, pp. 4038–4051, June 2017.
- [27] J. Mo and R. W. Heath, "High SNR capacity of millimeter wave MIMO systems with one-bit quantization," in *2014 Information Theory and Applications Workshop (ITA)*, February 2014, pp. 1–5.
- [28] S. Jacobsson, G. Durisi, M. Coldrey, U. Gustavsson, and C. Studer, "One-bit massive MIMO: Channel estimation and high-order modulations," in *2015 IEEE International Conference on Communication Workshop (ICCW)*, June 2015, pp. 1304–1309.
- [29] J. Choi, J. Mo, and R. W. Heath, "Near Maximum-Likelihood Detector and Channel Estimator for Uplink Multiuser Massive MIMO Systems With One-Bit ADCs," *IEEE Transactions on Communications*, vol. 64, no. 5, pp. 2005–2018, May 2016.

- [30] C. Mollén, J. Choi, E. G. Larsson, and R. W. Heath, "Performance of Linear Receivers for Wideband Massive MIMO with One-Bit ADCs," in *WSA 2016; 20th International ITG Workshop on Smart Antennas*, March 2016.
- [31] —, "Uplink Performance of Wideband Massive MIMO With One-Bit ADCs," *IEEE Transactions on Wireless Communications*, vol. 16, no. 1, pp. 87–100, January 2017.
- [32] Y. Li, C. Tao, L. Liu, G. Seco-Granados, and A. L. Swindlehurst, "Channel estimation and uplink achievable rates in one-bit massive MIMO systems," in *2016 IEEE Sensor Array and Multichannel Signal Processing Workshop (SAM)*, July 2016.
- [33] Y. Li, C. Tao, L. Liu, A. Mezghani, and A. L. Swindlehurst, "How Much Training Is Needed in One-Bit Massive MIMO Systems at Low SNR?" in *2016 IEEE Global Communications Conference (GLOBECOM)*, December 2016.
- [34] Y. Li, C. Tao, G. Seco-Granados, A. Mezghani, A. L. Swindlehurst, and L. Liu, "Channel Estimation and Performance Analysis of One-Bit Massive MIMO Systems," *IEEE Transactions on Signal Processing*, vol. 65, no. 15, pp. 4075–4089, August 2017.
- [35] R. Q. Twiss, "Nyquist's and Thevenin's Theorems Generalized for Nonreciprocal Linear Networks," *Journal of Applied Physics*, vol. 26, no. 5, pp. 599–602, May 1955.
- [36] K. Rohlfs and T. L. T. L. Wilson, *Tools of Radio Astronomy*. Berlin:Springer, 2004.
- [37] M. Franceschetti, *Wave Theory of Information*. Cambridge University Press, 2017.
- [38] A. Mezghani and A. L. Swindlehurst, "mmWave massive MIMO with simple RF and appropriate DSP," in *2017 51st Asilomar Conference on Signals, Systems, and Computers*, 2017, pp. 277–284.
- [39] A. Mezghani and J. A. Nossek, "Capacity lower bound of MIMO channels with output quantization and correlated noise," in *IEEE International Symposium on Information Theory Proceedings (ISIT)*, 2012.
- [40] A. K. Saxena, A. Mezghani, R. W. Heath, and J. G. Andrews, "Linear Transmit Precoding with Optimized Dithering," in *2019 53rd Asilomar Conference on Signals, Systems, and Computers*, 2019, pp. 838–842.
- [41] A. K. Saxena, A. Mezghani, and R. W. Heath, "Linear CE and 1-bit quantized precoding with optimized dithering," *IEEE Open Journal of Signal Processing*, December 2020.
- [42] E. Kokiopoulou and Y. Saad, "Orthogonal Neighborhood Preserving Projections: A Projection-Based Dimensionality Reduction Technique," *IEEE Transactions on Pattern Analysis and Machine Intelligence*, vol. 29, no. 12, pp. 2143–2156, 2007.